

## Rapid, Scalable Construction of Highly Crystalline Acylhydrazone Two-dimensional Covalent Organic Frameworks via Dipole-Induced Antiparallel Stacking

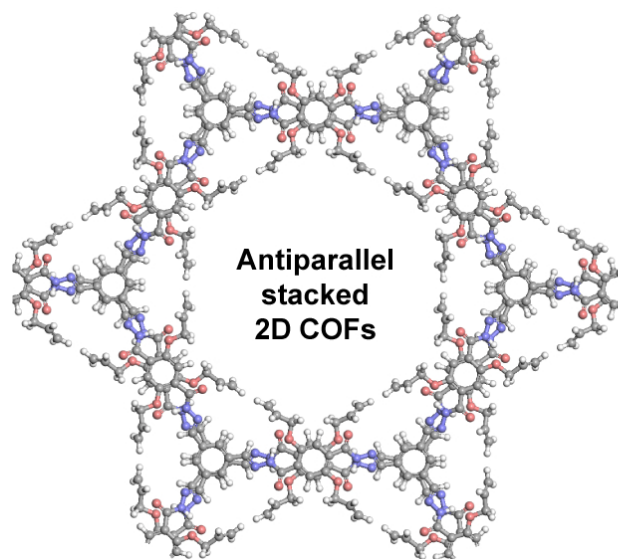
Xing Li, Jingsi Qiao, See Wee Chee, Hai-Sen Xu, Xiaoxu Zhao, Hwa Seob Choi, Wei Yu, Su Ying Quek, Utkur Mirsaidov, and Kian Ping Loh

*J. Am. Chem. Soc.*, **Just Accepted Manuscript** • DOI: 10.1021/jacs.0c00553 • Publication Date (Web): 20 Feb 2020

Downloaded from [pubs.acs.org](https://pubs.acs.org) on February 22, 2020

### Just Accepted

“Just Accepted” manuscripts have been peer-reviewed and accepted for publication. They are posted online prior to technical editing, formatting for publication and author proofing. The American Chemical Society provides “Just Accepted” as a service to the research community to expedite the dissemination of scientific material as soon as possible after acceptance. “Just Accepted” manuscripts appear in full in PDF format accompanied by an HTML abstract. “Just Accepted” manuscripts have been fully peer reviewed, but should not be considered the official version of record. They are citable by the Digital Object Identifier (DOI®). “Just Accepted” is an optional service offered to authors. Therefore, the “Just Accepted” Web site may not include all articles that will be published in the journal. After a manuscript is technically edited and formatted, it will be removed from the “Just Accepted” Web site and published as an ASAP article. Note that technical editing may introduce minor changes to the manuscript text and/or graphics which could affect content, and all legal disclaimers and ethical guidelines that apply to the journal pertain. ACS cannot be held responsible for errors or consequences arising from the use of information contained in these “Just Accepted” manuscripts.



6 examples  
High crystallinity  
 $\text{FWHM}_{100} \geq 0.25^\circ$   
Fast production in 30 min  
One-pot yield up to 1.4 g

24  
25  
26  
27  
28  
29  
30  
31  
32  
33  
34  
35  
36  
37  
38  
39  
40  
41  
42  
43  
44  
45  
46  
47  
48  
49  
50  
51  
52  
53  
54  
55  
56  
57  
58  
59  
60

TOC

# Rapid, Scalable Construction of Highly Crystalline Acylhydrazone Two-dimensional Covalent Organic Frameworks *via* Dipole-Induced Antiparallel Stacking

Xing Li<sup>#,†</sup>, Jingsi Qiao<sup>#,‡</sup>, See Wee Chee<sup>§,⊥</sup>, Hai-Sen Xu<sup>†</sup>, Xiaoxu Zhao<sup>||</sup>, Hwa Seob Choi<sup>†</sup>, Wei Yu<sup>†</sup>, Su Ying Quek<sup>‡,§</sup>, Utkur Mirsaidov<sup>§,⊥</sup>, Kian Ping Loh<sup>†,\*</sup>

<sup>†</sup>Department of Chemistry, National University of Singapore, 3 Science Drive 3, Singapore 117543, Singapore.

<sup>‡</sup>Centre for Advanced 2D Materials and Graphene Research Centre, National University of Singapore, 6 Science Drive 2, Singapore 117546, Singapore.

<sup>§</sup>Department of Physics, National University of Singapore, 2 Science Drive 3, Singapore 117551, Singapore.

<sup>⊥</sup>Centre for BioImaging Sciences, Department of Biological Sciences, National University of Singapore, 14 Science Drive 4, Singapore 117557, Singapore.

<sup>||</sup>Department of Materials Science and Engineering, National University of Singapore, 9 Engineering Drive 1, Singapore 117575, Singapore.

<sup>#</sup>These authors contribute equally to this work.

\*Corresponding Author: [chmlohkp@nus.edu.sg](mailto:chmlohkp@nus.edu.sg)

## Abstract

Covalent organic frameworks are an emerging class of porous crystalline organic materials that can be designed and synthesized from the bottom up. Despite progress made in synthesizing COFs of diverse topologies, the synthesis methods are often tedious and unscalable, hampering practical applications. Herein, we demonstrate a scalable, robust method to produce highly crystalline acylhydrazone two-dimensional (2D) COFs with diversified structures (6 examples) under open and stirred conditions, with growth typically completed in only 30 mins. Our strategy involves selecting molecular building blocks that have bond dipole moments with spatial orientations that favour antiparallel stacking, and whose structure allows restriction of intramolecular bond rotation (RIR) via intra- and interlayer hydrogen bonding. This method is widely applicable for hydrazide linkers containing various sidechain functionalities and toxicities. By this strategy, the gram-scale synthesis of two highly crystalline COFs (up to 1.4 g yield) were obtained in a one-pot reaction within 30 min.

## Introduction

The invention of covalent organic frameworks (COFs) is yet another proof of mankind's ability to control matter, whereby small organic molecular building units can be extended into highly ordered, porous frameworks via strong covalent interactions.<sup>1-6</sup> Extensive research has been conducted to construct COFs with different topologies, ranging from two-<sup>7-8</sup> and three-dimensional<sup>9-10</sup> (2D and 3D, respectively) to interwoven structures<sup>11-12</sup>. COFs find use in a wide variety of applications, such as gas separation,<sup>13-15</sup> energy storage,<sup>16-18</sup> emission,<sup>19-22</sup> catalysis,<sup>23-27</sup> ion conduction<sup>28-32</sup> and nonlinear optics<sup>33-34</sup>. Despite considerable advances, the practical application of COFs is hampered by a lack of scalable synthesis methods. The challenging aspect of COF synthesis is that the crystallization process competes with the more facile polymerization process. To suppress random polymerization, the crystallization process must proceed under self-correcting conditions, where the bonds can be dynamically repaired. This is necessary to minimize defects and to form crystalline materials.<sup>35-36</sup> Currently, the growth of highly crystalline COFs usually takes from 3–7 days to more than a month under sealed, undisturbed conditions, and only limited quantities (<100 mg) can be synthesized at any one time.<sup>10, 37-38</sup> Dichtel *et al.* demonstrated the fast crystallization of COF-5 in 2014<sup>39</sup>, which culminated in the synthesis of micrometer-size single crystals in 2018<sup>8</sup>. Dichtel and co-worker also reported the fast growth of imine COFs using metal triflates as catalyst<sup>40</sup>. In 2017, Banerjee *et al.* demonstrated the fast production of a series of ultraporous  $\beta$ -ketoenamine COFs using *p*-toluenesulfonic acid as the catalyst *via* an organic terracotta process<sup>41</sup>. In 2018, Fang *et al.* reported the ambient-condition synthesis of 3D imine COFs within 12 h using ionic liquids as solvents<sup>42</sup>. Due to the mutual exclusion of high crystallinity and fast growth for most COFs, there are still plenty of room for improving the design of the building blocks to ensure fast crystallization without compromising the

1  
2  
3 crystallinity of COFs. To date, the fast crystallization of COFs has only been achieved for  
4 boronate<sup>39</sup>, imine<sup>40</sup> and  $\beta$ -ketoenamine<sup>41</sup> COFs, and not reported for hydrazone COFs.  
5  
6  
7

8  
9 Currently, the most reliable way to synthesize COFs is through freeze-pump-thaw techniques  
10 and under sealed solvothermal conditions, which are not cost-effective for scalable  
11 production. Therefore, there is a need for a robust and cost-effective method to produce high-  
12 quality COFs beyond the laboratory scale. Yaghi and coworkers developed hydrazone-linked  
13 COFs in 2011<sup>43</sup>, which have shown great potential in wide ranging applications such as  
14 catalysis<sup>44-45</sup>, sensing<sup>46</sup>, gas storage<sup>14, 47</sup>, light emission<sup>19</sup>, ion conduction<sup>48</sup>, metal gas  
15 batteries<sup>49</sup>. Hydrazone-linked COFs are potentially suitable for large scale production due to  
16 the ease of synthesizing hydrazide building units. However, the structures of hydrazone COFs  
17 reported to date are rather limited and the reported synthesis time typically requires three  
18 days<sup>43, 45-46</sup>. Herein, we report a rapid, scalable production of highly crystalline 2D  
19 acylhydrazone COFs via acylhydrazide linkers with different sidechain functionalities,  
20 topicities and geometries under robust, stirred conditions. Our strategy is based on the  
21 following hypothesis: since a self-correction process is the rate-determining step for  
22 obtaining highly crystalline COFs, the key to achieving high rate of crystallization lies in  
23 minimizing error. The major source of error during 2D COF growth is attributed to  
24 hyperbranching owing to rotation of molecular bonds in the building units (Figure 1A), as  
25 well as random stacking owing to the small energy differences between different stacking  
26 order. Our rapid crystallization strategy is based on using molecular building blocks with  
27 intra- and interlayer hydrogen bonding and dipole-induced antiparallel stacking of the COF  
28 layers (Figure 1B). Intralayer hydrogen bonding was demonstrated by Banerjee *et al.* to  
29 enhance the crystallinity and stability of porphyrin COFs in 2013<sup>50</sup>. In 2015, Jiang *et al.*  
30 demonstrated the intralayer hydrogen bonding is beneficial for the crystallinity, physical  
31 properties and photochemical activity of porphyrin COFs<sup>51</sup>. The importance of intralayer  
32  
33  
34  
35  
36  
37  
38  
39  
40  
41  
42  
43  
44  
45  
46  
47  
48  
49  
50  
51  
52  
53  
54  
55  
56  
57  
58  
59  
60

1  
2  
3 hydrogen bonding for enhancing COF crystallinity was further reported by Ma *et al.* in  
4  
5 2018<sup>52</sup>. In 2018, Banerjee and co-workers showed that interlayer hydrogen bonding could  
6  
7 dramatically enhance the chemical stability of a series of fast-synthesized  $\beta$ -ketoenamine  
8  
9 COFs against extremely harsh environments such as concentrated sulfuric acid<sup>53</sup>. There has  
10  
11 been no systematic study of how electrostatic interactions in antiparallel stacking, as well as  
12  
13 intra- and intermolecular hydrogen bonding, can be incorporated into the building blocks to  
14  
15 speed up the crystallization of COF. In fact, our experiments and Density functional theory  
16  
17 (DFT) calculations show that the combination of dipole-induced antiparallel stacking, intra-  
18  
19 and interlayer hydrogen bonding are essential for fast growth in acylhydrazone COFs (Figure  
20  
21  
22  
23  
24 S1).  
25  
26  
27  
28  
29  
30  
31  
32  
33  
34  
35  
36  
37  
38  
39  
40  
41  
42  
43  
44  
45  
46  
47  
48  
49  
50  
51  
52  
53  
54  
55  
56  
57  
58  
59  
60

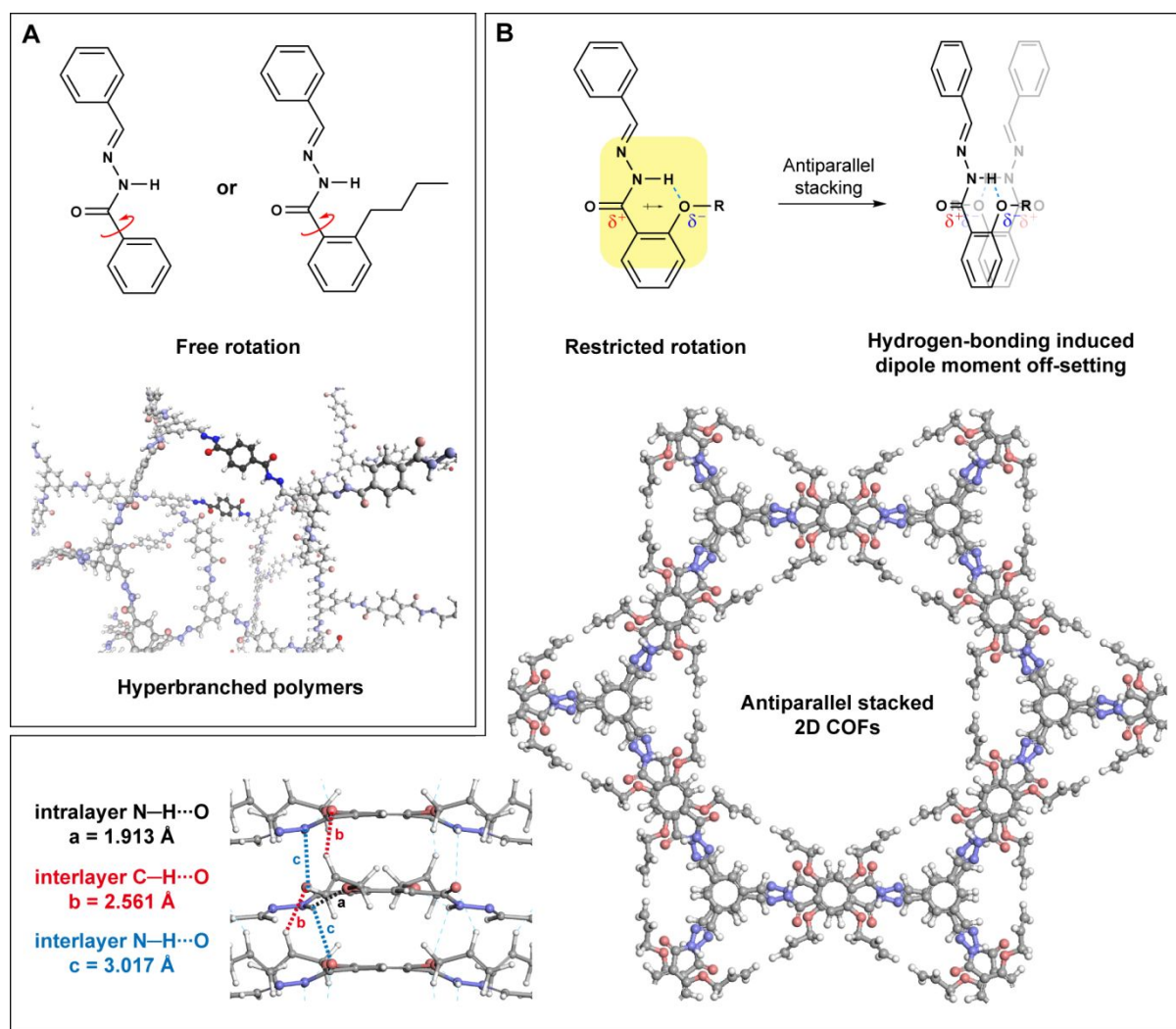
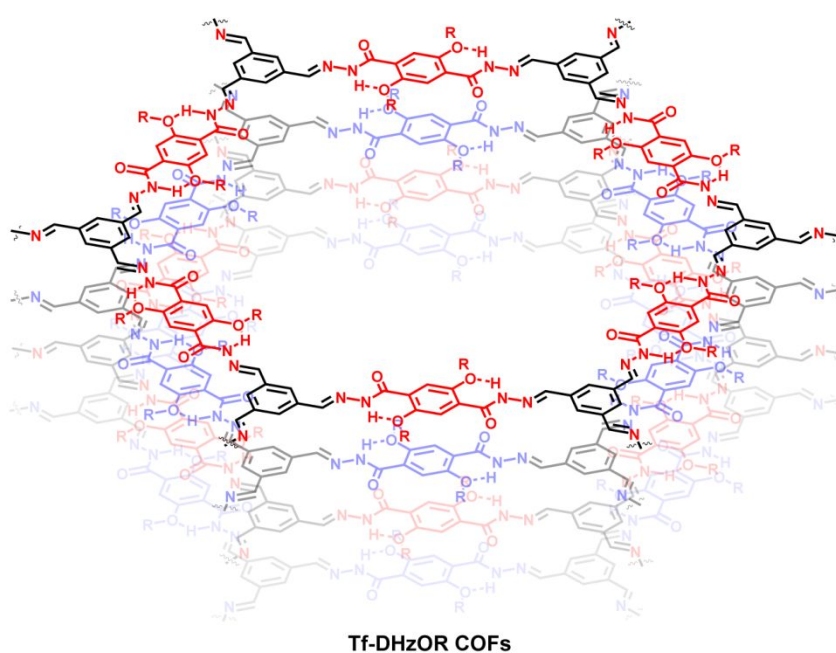
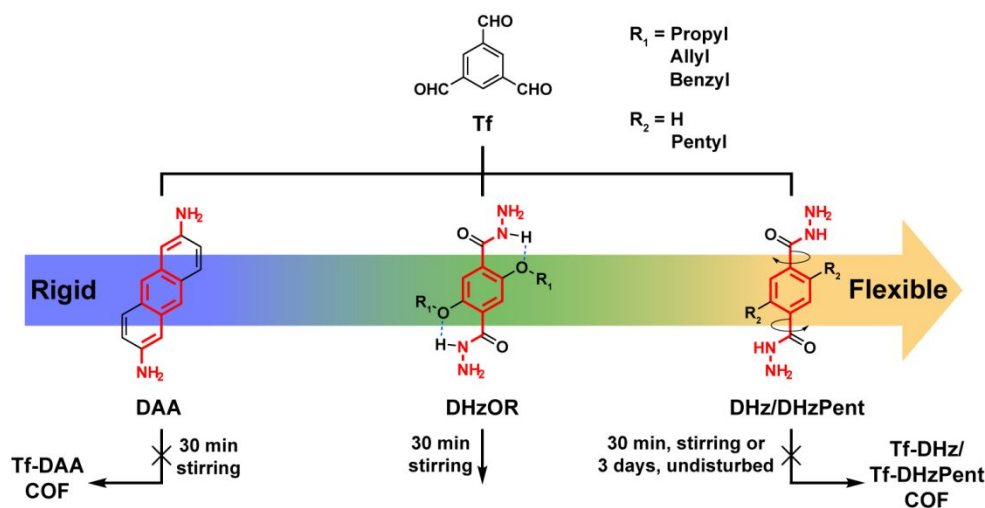


**Figure 1. Ultrafast growth of highly crystalline COFs via dipole-induced antiparallel stacking.** (A) Formation of amorphous polymers from rotationally unrestricted building units. Due to the free intramolecular bond rotation, the covalent extension of the building unit is not confined in 2D space, leading to hyperbranched 3D polymers. (B) COF formation via rotationally regulated synthesis. DFT-optimized COF exhibits antiparallel stacking. Intramolecular hydrogen bond restricts bond rotation, confining the formation of covalent linkages in 2D space; the intermolecular hydrogen bond further limits the random sliding of each of the COF layers, leading to a periodic stacked structure.

## Results and Discussion

To access both intra- and interlayer hydrogen bonding in the COF system for fast crystallization, we expect that both in-plane rigidity and out-of-plane flexibility is required for the building blocks. To prove this hypothesis, we attempted to prepare COFs from three isorecticular structures with different degrees of rotational freedom (Figure 2) under standard

1  
2  
3 solvothermal growth conditions. Three isorecticular materials were synthesized using three  
4 types of building units having highly similar geometry but different rigidities, and with the  
5 commonly used 1,3,5-triformylbenzene (**Tf**) as the linker. Anthracene-2,6-diamine (**DAA**)  
6 has the highest number of bonds frozen in the fused benzene rings of the backbone; thus, it is  
7 the most rigid among the three types of building units used. Terephthalohydrazide (**DHz**) or  
8 2,5-dipentylterephthalohydrazide (**DHzPent**), which is incapable of hydrogen bonding, is the  
9 most flexible building unit among the three. 2,5-Dialkyloxyterephthalohydrazide (**DHzOR**,  
10 R = propyl, allyl, and benzyl) possesses both rigidity and flexibility due to regulated bond  
11 rotation via intramolecular hydrogen bonding in a six-membered ring. Powder X-ray  
12 diffraction (PXRD) analysis is used for crystallinity confirmation and structural  
13 determination of COFs. Here, we use the full width at half-maximum (FWHM) of the  
14 strongest (100) peak to determine the quality of the COF crystals, which was estimated by the  
15 Bruker software diffraceva-v5.1. Under standard solvothermal growth conditions,  
16 condensation of **Tf** and **DHz/DHzPent** only affords amorphous products (Figures S4 and S5,  
17 respectively), suggesting that a highly flexible building unit with unconstrained bond rotation  
18 reduces crystallinity. Meanwhile, Schiff-base condensation of **Tf** and **DAA** affords COFs  
19 with good-to-moderate crystallinity ( $\text{FWHM}_{100} = 0.49\text{--}0.69^\circ$ ) under standard long-duration  
20 solvothermal growth conditions (Figure S3), indicating that restriction of molecular bond  
21 rotation is beneficial for COF growth. Using **Tf** and **DHzOR** (R = Pr, All, or Bn), hydrazone  
22 COFs with different sidechain functionalities, including propoxy, allyloxy, and benzyloxy,  
23 were also successfully synthesized (Figure S6). When grown under standard long-duration  
24 condition, the isolated Tf-DHzOR COF products exhibit excellent crystallinity with intense  
25 PXRD peaks and  $\text{FWHM}_{100}$  values of 0.36, 0.25, and  $0.56^\circ$  for Tf-DHzOPr, Tf-DHzOAll,  
26 and Tf-DHzOBn, respectively.  
27  
28  
29  
30  
31  
32  
33  
34  
35  
36  
37  
38  
39  
40  
41  
42  
43  
44  
45  
46  
47  
48  
49  
50  
51  
52  
53  
54  
55  
56  
57  
58  
59  
60



41  
42  
43  
44  
45  
46  
47  
48

**Figure 2. Rotationally regulated synthesis of 2D COFs.** Three isorecticular structures were synthesized based on building units with different degrees of bond rotation restriction under ultrafast or undisturbed prolonged conditions. Only DHzOR units, with moderate rigidity and flexibility, enjoy the ultrafast synthesis method, affording antiparallel stacked highly crystalline COFs.

49  
50  
51  
52  
53  
54  
55  
56  
57  
58  
59  
60

Next, the effect of bond rotation restriction in enhancing crystallization was tested by growing COFs under ultrafast and robust conditions. In a simple set-up (Figure S2), the building units were heated under stirring in air for 30 min in different solvents using concentrated acetic acid as the catalyst. Both **DAA** and **DHz/DHzPent** afforded amorphous polymers upon condensation with **Tf**, suggesting insufficient time for self-correction (Figures

1  
2  
3 S3, S7, and S8). The FT-IR spectra of Tf-DHzOR prepared under ultrafast robust conditions  
4  
5 are consistent with those prepared for longer times, suggesting that the polymerization of Tf-  
6  
7 DHzOR was completed in 30 min (Figure S9). To our delight, condensations of Tf and the  
8  
9 **DHzOR** species afford highly homogeneous and crystalline COFs, as confirmed by the  
10  
11 intense PXRD peaks with the narrow FWHM<sub>100</sub> (Figures 3). This suggests that the restriction  
12  
13 of bond rotation via intra- and interlayer hydrogen bonding is an efficient method to shorten  
14  
15 the time needed for crystallization. Besides, this method can be used to produce high-quality  
16  
17 COFs bearing propoxy, allyloxy, and benzyloxy sidechain functionalities with narrow XRD  
18  
19 FWHM<sub>100</sub> values of 0.32°, 0.33°, and 0.48°, respectively (Figure 3), indicating good  
20  
21 tolerance to variable sidechain functionalities. The high tolerance of sidechain functionalities  
22  
23 suggests the great value of this type of COF for application-led design of the materials.  
24  
25  
26  
27  
28

29  
30 PXRD patterns exhibited the most intense peaks at 3.41°, 3.37°, and 3.27° for the fast-  
31  
32 produced Tf-DHzOPr, Tf-DHzOAll, and Tf-DHzOBn, respectively, corresponding to their  
33  
34 (100) facets. Tf-DHzOPr showed another four peaks at 5.93°, 6.91°, 9.18°, and 26.43°,  
35  
36 corresponding to the (110), (200), (210), and (001) facets. Similarly, Tf-DHzOAll displayed  
37  
38 another four peaks at 5.93°, 6.85°, 9.12°, and 26.43°, corresponding to the (110), (200), (210),  
39  
40 and (001) facets. Tf-DHzOBn exhibited another three peaks at 6.60°, 8.77°, and 25.67°,  
41  
42 corresponding to the (200), (210), and (001) facets. Structures based on antiparallel, eclipsed  
43  
44 and staggered stacking have been simulated for the three COFs (Figures S11–13). The PXRD  
45  
46 patterns of antiparallel and eclipsed structures agree well with experiments. To further  
47  
48 confirm the COF structures, we grew the single crystals of model compounds and performed  
49  
50 DFT simulations. The single crystal structures of the model compounds revealed that the  
51  
52 intra-molecular hydrogen bonded fragments exhibited antiparallel packing, while the non-  
53  
54 hydrogen bonded molecules show parallel packing (Figure S11). This suggests that  
55  
56 intramolecular hydrogen bonding facilitates antiparallel stacking, which may be explained by  
57  
58  
59  
60

1  
2  
3 the fact that restriction of bond rotation increases in-plane rigidity and allows the bond dipole  
4 moments due to C( $\delta^+$ )=O( $\delta^-$ ) and O( $\delta^-$ )-R( $\delta^+$ ) to spatially orient in the in-plane direction.  
5  
6 This allows strong dipole-dipole interaction with the antiparallel stacked layers. Moreover,  
7  
8 simulation revealed the total energy of DFT-optimized antiparallel stacked Tf-DHzOAll are  
9  
10 3.07 eV per unit cell (containing two layers) more stable than the eclipsed stacked (Table S1).  
11  
12 Besides, simulated structures based on DFT optimization or Universal force field calculation  
13  
14 exhibited a  $\pi$ - $\pi$  interlayer distance of 3.4~3.5 Å for antiparallel stacked structures in stark  
15  
16 contrast to 3.7~3.8 Å for eclipsed stacked structures<sup>46</sup>, where the former agrees well with our  
17  
18 experimental PXRD results. The DFT-optimized antiparallel stacked Tf-DHzOAll suggests  
19  
20 the existence of interlayer hydrogen bonding between the acyl oxygen and the sidechain  
21  
22 hydrogen in the adjacent layer, which is consistent with the X-ray photoelectron spectroscopy  
23  
24 (XPS) and the solid-state <sup>13</sup>C NMR spectra. The O 1s spectra reveals the binding energy for  
25  
26 C=O shifts from 533.8 eV (non-hydrogen bonded Tf-DHz) to 533.2 eV (Tf-DHzOAll)  
27  
28 (Figure 4), indicating a change of chemical environment of the acyl oxygen due to interlayer  
29  
30 hydrogen bonding. Furthermore, solid-state <sup>13</sup>C NMR spectra reveal a chemical shift of acyl  
31  
32 carbon from 164.1 ppm (Tf-DHz) to 156.5 ppm (Tf-DHzOAll) (Figure S46). This is because  
33  
34 the interlayer hydrogen bonding in Tf-DHzOAll weakens the electron withdrawing ability of  
35  
36 the acyl oxygen, resulting in a stronger electron shielding of the acyl carbon and therefore the  
37  
38 upfield shift. In addition, we also compare the <sup>13</sup>C NMR spectra of Tf-DHzOAll COF and  
39  
40 DHzOAll model compound (Fig. S47). The chemical shift of the acyl carbon is at 161.42  
41  
42 ppm for the major DHzOAll model isomer, while it is at 156.5 ppm for Tf-DHzOAll COF.  
43  
44 This strongly suggests that COFs adopt antiparallel stacking to facilitate interlayer hydrogen  
45  
46 bonding involving acyl oxygen. The Pawley refinement based on antiparallel structures  
47  
48 displayed good consistency with the experimental PXRD patterns, with ( $R_p$ ,  $R_{wp}$ ) values of  
49  
50 (4.49%, 5.64%), (3.50%, 4.28%), and (2.46%, 3.08%) for Tf-DHzOPr, Tf-DHzOAll, and Tf-  
51  
52  
53  
54  
55  
56  
57  
58  
59  
60

DHzOBn, respectively. The Tf-DHzOR COFs all adopt antiparallel stacking with Pawley refined cells belonging to the  $P6CC$  space group and cell parameters of  $a = b = 29.62 \text{ \AA}$ ,  $c = 6.98 \text{ \AA}$  for Tf-DHzOPr,  $a = b = 29.86 \text{ \AA}$ ,  $c = 7.07 \text{ \AA}$  for Tf-DHzOAll, and  $a = b = 30.18 \text{ \AA}$ ,  $c = 7.04 \text{ \AA}$  for Tf-DHzOBn.

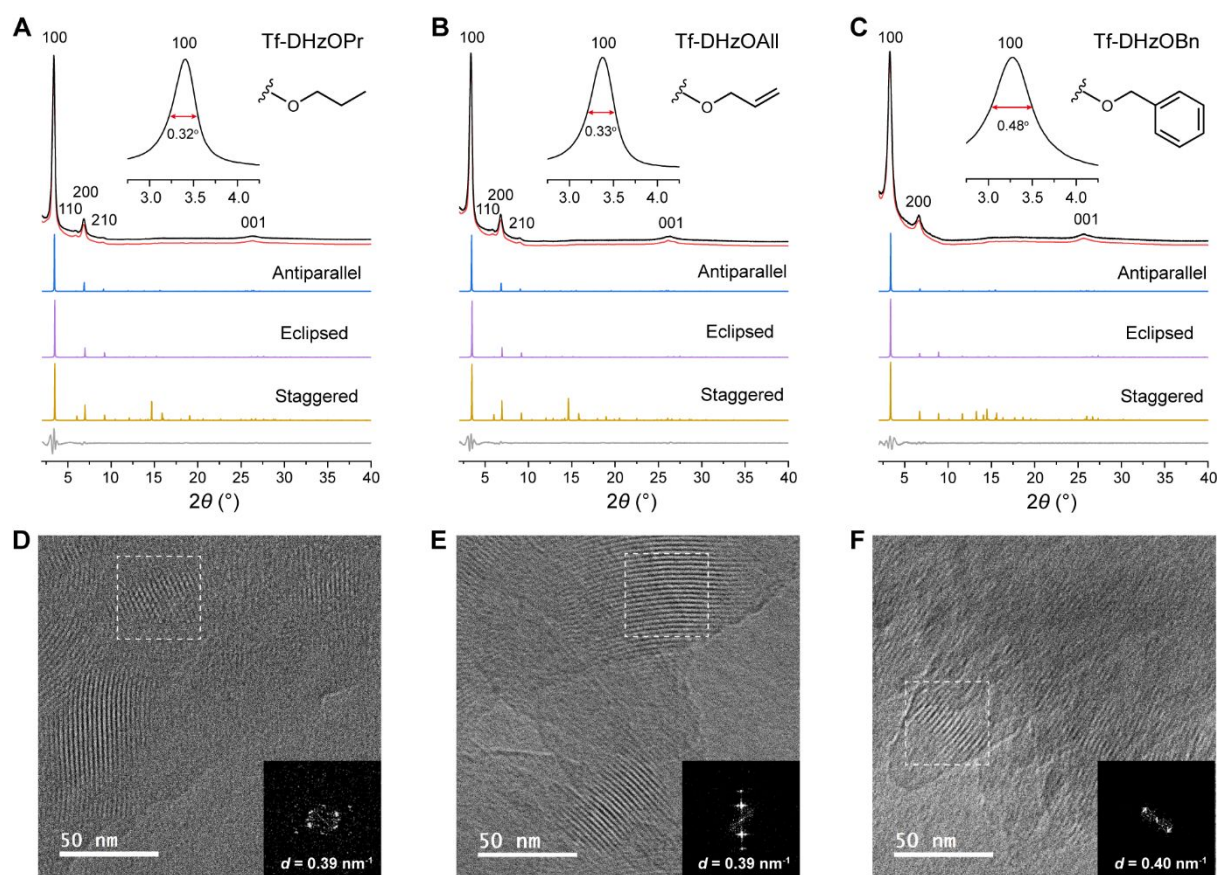


**Figure 3. PXRD patterns and TEM images of the as-synthesized COFs with ditopic building units.** PXRD characterization of (A) Tf-DHzOPr COF with propoxy sidechain, (B) Tf-DHzOAll COF with allyloxy sidechain, and (C) Tf-DHzOBn COF with benzyloxy sidechain (black: experimental; red: Pawley-refined; blue: simulated antiparallel stacking; purple: simulated eclipsed stacking; yellow: simulated staggered stacking; grey: difference between experimental and Pawley-refined PXRD patterns). TEM images of (D) Tf-DHzOPr COF (E) Tf-DHzOAll COF, and (F) Tf-DHzOBn COF. The sample was imaged under low temperature with liquid nitrogen cooling (Inset: FFT of the lattice fringes).

The low-dose cryogenic transmission electron microscopy (TEM) also confirmed the good crystallinity of the COFs obtained under ultrafast conditions (Figure 3D-F). The fast Fourier transform (FFT) of the lattice fringes suggests  $d$ -spacings of 25.4, 25.5 and 25.0  $\text{\AA}$  for Tf-

1  
2  
3 DHzOPr, Tf-DHzOAll and Tf-DHzOBn, respectively, which are consistent with the *d*-  
4 spacings of 25.9, 26.2, and 27.0 Å derived from PXRD patterns of the (100) facets for Tf-  
5 DHzOPr, Tf-DHzOAll and Tf-DHzOBn, respectively.  
6  
7  
8  
9

10 The quality of COFs obtained via ultrafast synthesis was further evaluated by nitrogen  
11 sorption experiments at 77 K (Figures S15 and S17). The sorption isotherms exhibited mainly  
12 type-I adsorption profiles with abrupt increases at  $P/P_0 < 0.1$ , indicating the microporosity of  
13 the materials. The Brunauer–Emmett–Teller (BET) surface areas of Tf-DHzOPr and Tf-  
14 DHzOAll were 701 and 501 m<sup>2</sup> g<sup>-1</sup> respectively, comparable to the corresponding values of  
15 747 and 461 m<sup>2</sup> g<sup>-1</sup> obtained for COFs synthesized over longer periods (Figures S15 and S17).  
16  
17 Compared to these, Tf-DHzOBn has a lower BET surface area of between 163 to 254 m<sup>2</sup> g<sup>-1</sup>,  
18 which is due to the bulky benzyl groups on the pore walls. Based on non-localized density  
19 functional theory (NLDFT) calculation, the pore widths have the greatest distributions  
20 centred at 1.69, 1.69, and 1.42 nm for Tf-DHzOPr, Tf-DHzOAll, and Tf-DHzOBn  
21 respectively, indicating good uniformity of pores. The hysteresis in the isotherms suggest  
22 there are also mesopores in the COFs, this is due to the flexible sidechains on the pore walls,  
23 which cause capillary condensation of the gas adsorbed.  
24  
25  
26  
27  
28  
29  
30  
31  
32  
33  
34  
35  
36  
37  
38  
39  
40  
41  
42  
43  
44  
45  
46  
47  
48  
49  
50  
51  
52  
53  
54  
55  
56  
57  
58  
59  
60

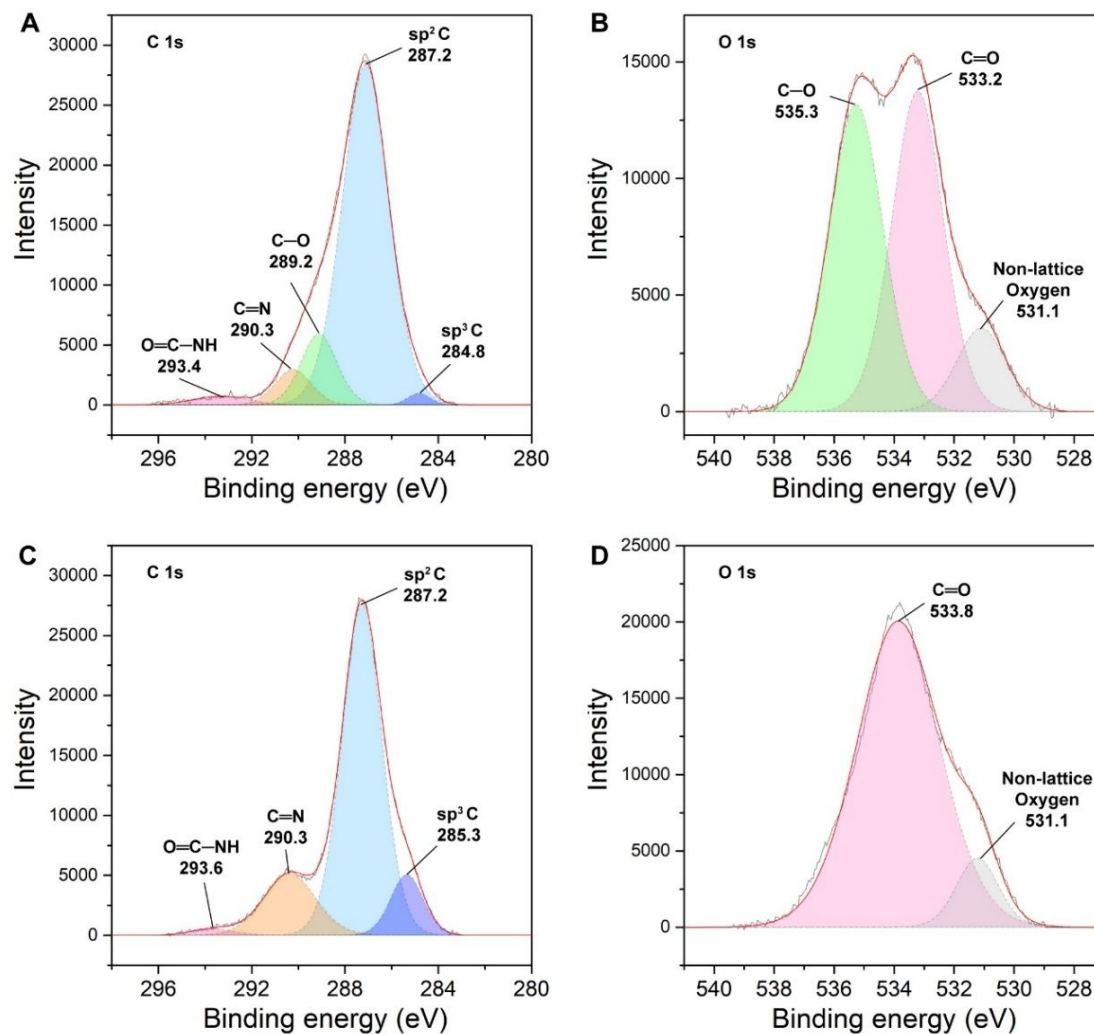


**Figure 4.** XPS spectra of Tf-DHzOAll COF and Tf-DHz. (A) C 1s spectrum of Tf-DHzOAll. (B) O 1s spectrum of Tf-DHzOAll. (C) C 1s spectrum of Tf-DHz. (D) O 1s spectrum of Tf-DHz.

The structural key to achieving ultrafast synthesis of highly crystalline COFs is the intramolecular N-H $\cdots$ O bonding formed in a six-membered ring in the alkyloxy-substituted hydrazide system. This molecular scaffold is fundamental to the construction of intra- and interlayer hydrogen bonding in 2D COFs, as well as facilitating dipole-dipole interactions in antiparallel stacked configurations. First, intralayer hydrogen bonding helps restrict molecular bond rotation and rigidifies the structure, confining the covalent extension of COF to a 2D plane. Second, the in-plane rigidity allows the bond dipole moments to lie in-plane, facilitating antiparallel stacking between the COF layers to minimize the total energy. Thirdly,

1  
2  
3 the interlayer hydrogen bonding between the acyl oxygen and the sidechain/hydrazone  
4 linkage from adjacent layers prevent the layers from sliding out of alignment and generating  
5 stacking faults. The interplay between different degrees of intra- and interlayer hydrogen  
6 bonding modulate the rigidities of the COF layers, leading to high structural adaptability for  
7 fast crystallization. Therefore, a molecular scaffold with the ability for intralayer/interlayer H  
8 bonding should be a useful building block for the fast growth of 2D COF. Accordingly, we  
9 designed and synthesized a tritopic building unit, **THzOPr** (Figure 5). To construct network  
10 structures in COFs, the total topicity of the building units should be no less than 5. From the  
11 synthesis viewpoint, a tritopic hydrazide building unit is more versatile because both ditopic  
12 and tritopic aldehydes can be reacted with **THzOPr** to form COFs. Using the most common  
13 tritopic aldehyde **Tf** and ditopic aldehyde, terephthalaldehyde (**Df**), as examples, highly  
14 crystalline COFs can be produced in only 30 min *via* condensation between **THzOPr** and *C*<sub>3</sub>-  
15 symmetric **Tf**, or *C*<sub>2</sub>-symmetric **Df**, respectively. The PXRD patterns of Tf-THzOPr and Df-  
16 THzOPr COFs exhibit narrow FWHM<sub>100</sub> values of 0.30° and 0.28°, respectively, confirming  
17 their excellent crystallinities. Tf-THzOPr showed seven PXRD peaks at 4.61°, 7.97°, 9.31°,  
18 12.30°, 14.04°, 16.17°, and 25.41°, corresponding to the (100), (110), (200), (210), (300),  
19 (220), and (001) facets; Df-THzOPr displayed seven peaks at 2.32°, 4.06°, 4.69°, 6.25°, 8.50°,  
20 10.28°, and 25.79°, corresponding to the (100), (110), (200), (120), (130), (410), and (001)  
21 facets. Structures based on antiparallel, eclipsed and staggered stacking have been simulated  
22 for Tf-THzOPr and Df-THzOPr (Figures S20 and S21, respectively). The experimental  
23 PXRD patterns agreed well with the simulated antiparallel stacking ones. The Pawley  
24 refinement based on the antiparallel structures displayed good consistency with the  
25 experimental PXRD patterns, with (*R*<sub>p</sub>, *R*<sub>wp</sub>) values of (2.15%, 2.89%) and (3.81%, 5.03%)  
26 for Tf-THzOPr and Df-DHzOPr, respectively. Both COFs adopt antiparallel stacking with  
27  
28  
29  
30  
31  
32  
33  
34  
35  
36  
37  
38  
39  
40  
41  
42  
43  
44  
45  
46  
47  
48  
49  
50  
51  
52  
53  
54  
55  
56  
57  
58  
59  
60

Pawley-refined cell parameters of  $a = b = 21.75 \text{ \AA}$ ,  $c = 6.99 \text{ \AA}$  with the  $P3C1$  space group for Tf-THzOPr, and  $a = b = 43.86 \text{ \AA}$ ,  $c = 6.70 \text{ \AA}$  with the  $P6$  space group for Df-THzOPr.

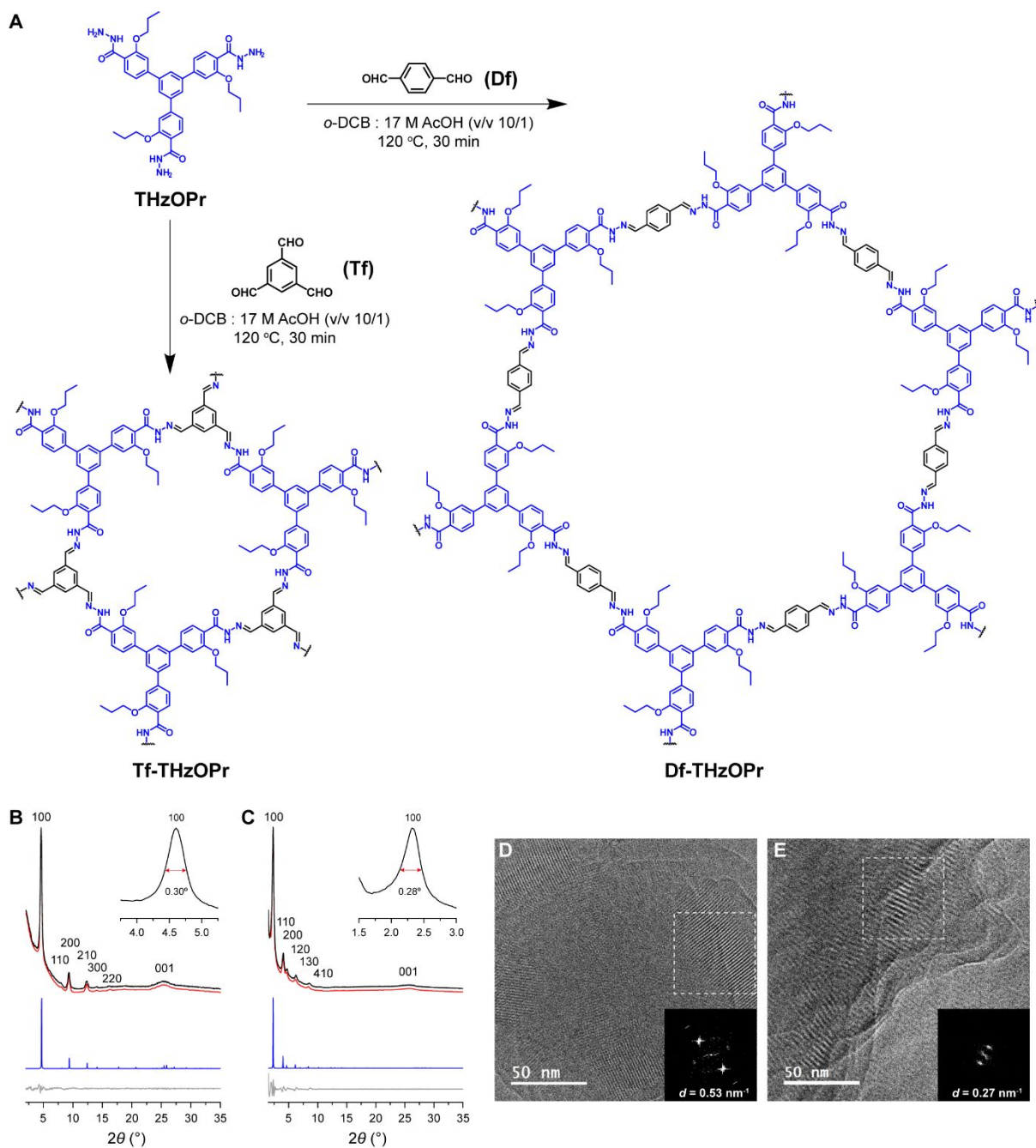


**Figure 5. Ultrafast synthesis of highly crystalline COFs with tritopic hydrazides.** A tritopic building unit with three sites of rotation regulation via hydrogen bonding, THzOPr, was designed and synthesized. Under ultrafast robust conditions, it can form highly crystalline COFs with linkers possessing different symmetries. (A) Synthesis of Tf-THzOPr and Df-THzOPr COFs. PXRD patterns of (B) Tf-THzOPr COF and (C) Df-THzOPr COF (black: experimental; red: Pawley-refined; blue: simulated eclipsed stacking; grey: difference of experimental and Pawley-refined PXRD). TEM images of (D) Tf-THzOPr COF and (E) Df-THzOPr COF. The sample was imaged under low temperature with liquid nitrogen cooling (Inset: FFT of the lattice fringes).

SEM images revealed highly uniform spherical morphologies for THzOPr COFs (Figures S35 and S36). The excellent crystallinity of THzOPr COFs was also verified by TEM (Figures 4D and E). The fast Fourier transform (FFT) of the lattice fringes suggests *d*-spacings of 19.0 and 37.3 Å for Tf-THzOPr and Df-THzOPr, respectively, which are consistent with the *d*-spacings of 19.2 and 38.1 Å derived from PXRD patterns of the (100) facets for Tf-THzOPr and Df-THzOPr respectively. Additionally, nitrogen sorption studies revealed a type-I isotherm for Tf-THzOPr COF and a type-IV isotherm for Df-THzOPr COF, typical for microporous and mesoporous materials, respectively (Figure S22). The estimated BET surface areas were 842 and 595 m<sup>2</sup> g<sup>-1</sup> for Tf-THzOPr COF and Df-THzOPr COF, respectively (Figure S23). The pore size calculation also reveals that the pores are uniformly distributed around 1.13 and 2.77 nm for Tf-THzOPr COF and Df-THzOPr, respectively, consistent with the simulated values. These results provide strong evidence that the restriction of bond rotation can be generalized to construct 2D COFs with diverse structures.

The ultrafast method under open, robust condition is desirable for large-scale production of high-quality COFs, and in principle can be scaled up to any amount depending on the requirement. As a proof of concept, we synthesized two highly crystalline COFs in gram scale under the ultrafast conditions, with one-pot yield of 1.4 g and 1.09 g for Tf-DHzOAll and Tf-DHzOPrY, respectively. The newly designed DHzOPrY building unit (blue colored molecule in Figure 6) possesses two acylhydrazide groups that are hydrogen bonded to the propoxy sidechains, and linked by an acetylene group. The PXRD patterns of Tf-DHzOPrY exhibit a narrow FWHM<sub>100</sub> of 0.24°, suggesting good crystallinity. Seven PXRD peaks were observed at 2.49°, 4.33°, 5.00°, 6.72°, 7.67°, 9.10° and 26.27°, which correspond to the (100), (110), (200), (210), (300), (310), and (001) facets, respectively. Antiparallel, eclipsed and staggered stacked Tf-DHzOPrY structures have been simulated (Figures S26). The experimental PXRD

1  
2  
3 patterns agreed well with the simulated antiparallel stacking one. The Pawley refinement  
4 based on the antiparallel structure displayed good consistency with the experimental PXRD  
5 patterns, with ( $R_p$ ,  $R_{wp}$ ) values of (3.59%, 4.64%) for Tf-DHzOPrY. The Tf-DHzOPrY COF  
6 adopts antiparallel stacking with Pawley-refined cells belong to the  $P6CC$  space group and  
7 cell parameters of  $a = b = 40.07 \text{ \AA}$ ,  $c = 6.94 \text{ \AA}$ . The nitrogen sorption studies reveal a typical  
8 type-IV isotherm for Tf-DHzOPrY, suggesting its mesoporosity. The BET surface area of Tf-  
9 DHzOPrY was estimated to be  $759 \text{ m}^2 \text{ g}^{-1}$ . According to the NLDFT calculation, the pore  
10 size distribution of Tf-DHzOPrY was localized at 2.66 nm, suggesting the uniformity of the  
11 pores.  
12  
13  
14  
15  
16  
17  
18  
19  
20  
21  
22  
23  
24  
25  
26  
27  
28  
29  
30  
31  
32  
33  
34  
35  
36  
37  
38  
39  
40  
41  
42  
43  
44  
45  
46  
47  
48  
49  
50  
51  
52  
53  
54  
55  
56  
57  
58  
59  
60

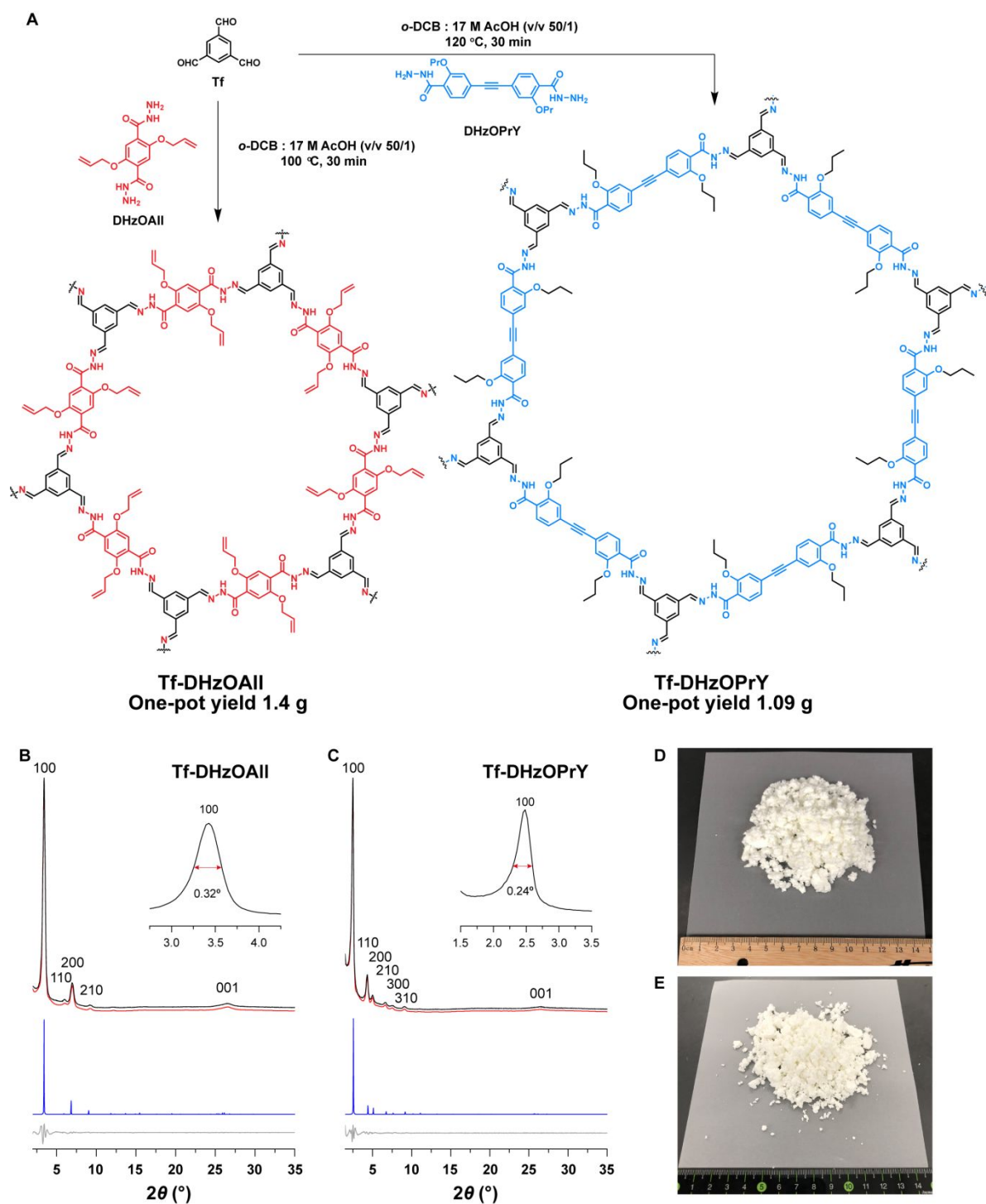


**Figure 6. Ultrafast one-pot synthesis of highly crystalline COFs in gram scale.** (A) Synthesis of Tf-DHzOAll and Tf-DHzOPrY COFs. PXRD patterns of (B) Tf-DHzOAll COF and (C) Tf-DHzOPrY COF (black: experimental; red: Pawley-refined; blue: simulated eclipsed stacking; grey: difference of experimental and Pawley-refined PXRD). Photo images of the gram-scale produced (D) Tf-DHzOAll COF and (E) Tf-DHzOPrY COF.

1  
2  
3 Since the dipole-induced antiparallel stacking and intra- and interlayer hydrogen bonding are  
4 essential for the restriction of molecular bond rotation in COF crystallization, disrupting these  
5  
6 should interfere with the crystallization of hydrazone COFs. To verify this, we grew Tf-  
7  
8 DHzOPr COF in various polar solvents with large dipole moment under the ultrafast  
9  
10 conditions (Figure S29). Polar solvent molecules with large dipole serve as hydrogen bond  
11  
12 acceptors, thus interfering with intra- and inter-molecular hydrogen bonding as well as the  
13  
14 dipole-induced antiparallel stacking. For COFs synthesized in aprotic non-polar solvents,  
15  
16 such as 1,2-dichlorobenzene (*o*-DCB) and mesitylene, PXRD patterns revealed that the  
17  
18 products are highly crystalline. In contrast, those prepared in polar solvents, such as 1,4-  
19  
20 dioxane and dimethyl sulfoxide (DMSO), showed poor to no crystallinity. Furthermore, we  
21  
22 studied the sidechain effect on the fast crystallization of COFs (Figure S30). COFs were  
23  
24 constructed using three different hydrazide building units (DHzOMe, DHzOEt, and  
25  
26 DHzOPrSEt) with different sidechains of methoxy, ethoxy and (ethylthio)propoxy,  
27  
28 representing various sidechain lengths. Under the ultrafast condition, Tf-DHzOMe did not  
29  
30 form COF; Tf-DHzOEt (COF-42) showed slight crystallinity; only Tf-DHzPrSEt (COF-  
31  
32 LZU8) exhibited high crystallinity. One explanation is that steric hindrance due to sidechains  
33  
34 reduces monomer rotation in the COFs, preventing hyperbranching. More importantly, DFT-  
35  
36 optimized COF structure suggests there is a significant interlayer hydrogen bonding between  
37  
38 the acyl oxygen and the hydrogen on the second carbon of the sidechain from adjacent layers  
39  
40 (Figure 1B and Figure S1). This explains why COF can be only fast crystallized when the  
41  
42 sidechain carbon number is no less than two. Therefore, both antiparallel stacking and  
43  
44 hydrogen bonding are critical for ultrafast robust synthesis of highly crystalline COFs.  
45  
46 Fortified by dipole-induced antiparallel stacking and hydrogen bonding, acylhydrazone COFs  
47  
48 exhibits good stability towards acid and base (Figure S31). The good crystallinity of Tf-  
49  
50 DHzOPr was retained after immersed in 1 M HCl or 1 M NaOH for 7 days. In contrast, the  
51  
52  
53  
54  
55  
56  
57  
58  
59  
60

1  
2  
3 crystallinity of Tf-DAA COF was badly degraded after immersing in 1 M HCl or 1 M NaOH  
4  
5 for only 1 day.  
6  
7

8 To obtain insights into how the crystallization of COFs is affected by hydrogen bonding, we  
9  
10 have carried out a series of DFT calculations. To investigate how intralayer hydrogen  
11  
12 bonding restricts bond rotation in COF layers, DFT simulations were conducted on  
13  
14 monolayer Tf-DHzPent, which are incapable of hydrogen bonding, and Tf-DHzOAll, which  
15  
16 can hydrogen-bond (Figure S45). The intralayer-hydrogen bonded COF monolayer exhibits a  
17  
18 planarized conformation and large rotational energy barrier against distortion, while the non-  
19  
20 hydrogen bonded COF monolayer displayed a contorted conformation with low rotational  
21  
22 energy barrier. We calculated the charge density map and interlayer differential charge  
23  
24 density of Tf-DHzOAll COF with antiparallel and eclipsed structures to study the effect of  
25  
26 stacking (Figure 7). In the eclipsed structure, electrostatic repulsion between electron-rich  
27  
28 groups prevents close-stacking (Figure 7B), resulting in weak interlayer interactions (Figure  
29  
30 7D). In contrast, antiparallel stacking avoids charge repulsion (Figure 7A) and instead allows  
31  
32 for electrostatic interactions between layers (Figure 7C). In the antiparallel structure, there is  
33  
34 a significant decrease of electron density on the acyl oxygen and the hydrogen on the second  
35  
36 carbon of the sidechain in the adjacent layer, and an increase of electron density on the outer  
37  
38 shell of the acyl oxygen, which is consistent with the interlayer hydrogen bonding.  
39  
40  
41  
42  
43  
44  
45  
46  
47  
48  
49  
50  
51  
52  
53  
54  
55  
56  
57  
58  
59  
60

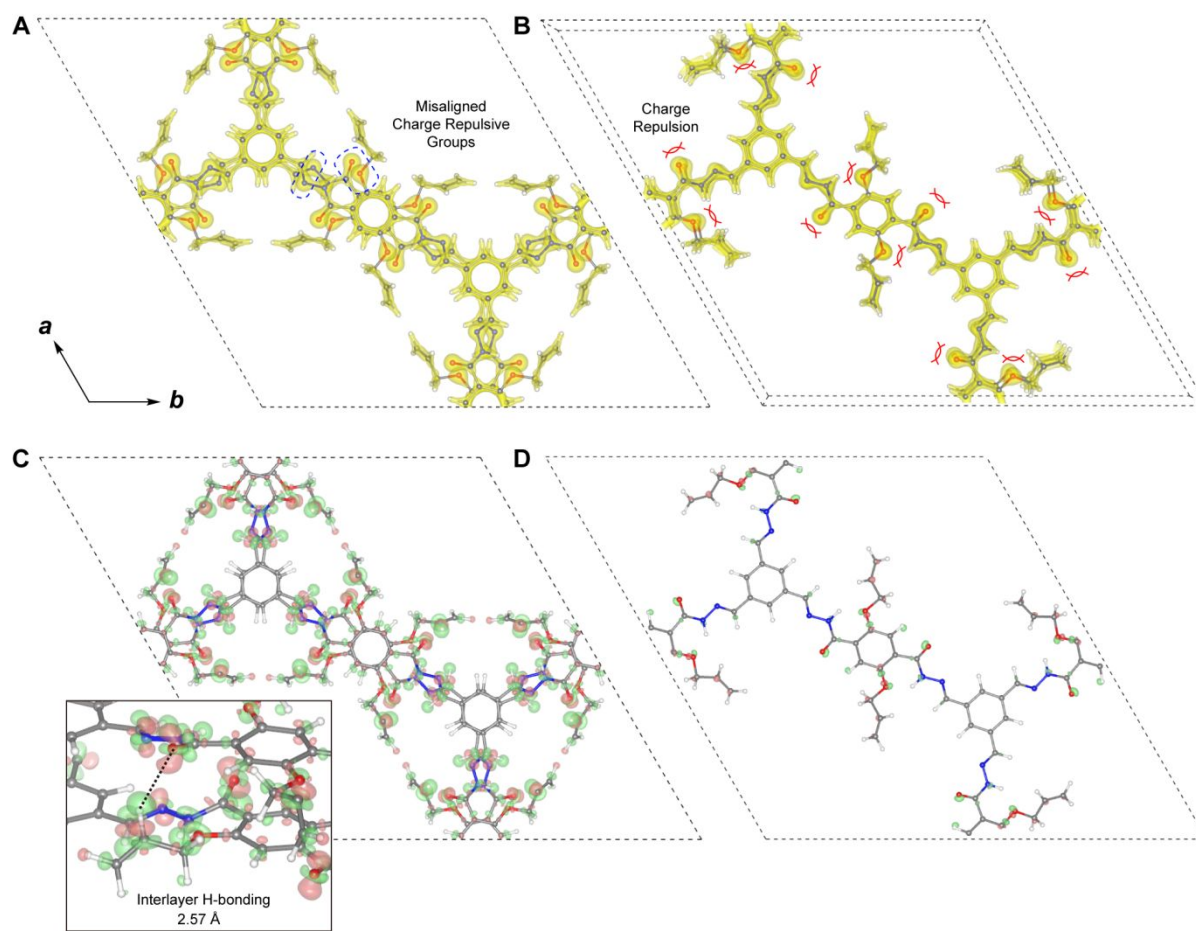


**Figure 7. Charge density of DFT-optimized Tf-DHzOAll COF with antiparallel and eclipse stacking.** (A) Total charge density of Tf-DHzOAll with antiparallel stacking. Electron-rich groups misalign to stabilize the system. (B) Total charge density of Tf-DHzOAll with eclipse stacking. Charge repulsion between the electron-rich units prevents close stacking. (C) Interlayer differential charge density of Tf-DHzOAll with antiparallel stacking. (D) Differential charge density of Tf-DHzOAll with eclipse stacking (Green: decrease of electron density; red: increase of electron density.) Total charge density (A and B) and differential charge density (C and D) are visualized using the isosurface of 0.25 and 0.001 e Bohr<sup>-3</sup>, respectively.

To conclude, we have demonstrated ultrafast synthesis of acylhydrazone 2D COFs under robust, scalable conditions. Systematic experimental studies and DFT calculations suggest that the ultrafast crystallization is underpinned by restriction of bond rotation by intramolecular hydrogen bonding, thus allowing dipole-dipole interactions between the molecular building blocks in the antiparallel stacked configuration, as well as interlayer hydrogen bonding. Using this approach, the gram-scale synthesis of structure-diversified acylhydrazone 2D COFs can be achieved in growth time as short as 30 min. In addition, the

1  
2  
3 synthetic scope can be extended to hydrazide building units with different geometries,  
4 sidechain functionalities and topologies. The ability to accelerate the synthesis of COFs,  
5 without compromising on crystalline quality, paves the way for large-scale applications of  
6 COFs.  
7  
8  
9  
10  
11  
12

## 13 **ASSOCIATED CONTENT**

### 14 **Supporting Information**

15  
16  
17  
18  
19 Supplementary material for this article is available. General information on instruments and  
20 methods; synthetic procedures; characterizations including PXRD, nitrogen sorption  
21 experiments, FTIR, solid-state <sup>13</sup>C NMR, SEM and TEM; study of solvent effect and  
22 sidechain length on COF growth; crystallite sizes and simulated BET surface areas; DFT-  
23 optimized COF structures; DFT simulation of monolayer COFs; single crystal file of model  
24 compounds; Scheme S1 to S4, Figure S1 to S47, Table S1 to S3.  
25  
26  
27  
28  
29  
30  
31  
32  
33

## 34 **AUTHOR INFORMATION**

### 35 **Corresponding Author**

36  
37  
38  
39  
40 \*Corresponding Author: [chmlhkp@nus.edu.sg](mailto:chmlhkp@nus.edu.sg)  
41  
42

### 43 **Notes**

44  
45  
46 #These authors contribute equally to this work.  
47  
48

### 49 **Acknowledgements**

50  
51 K.P.L., X.L., S.Y.Q. and J.Q. acknowledge NRF-CRP grant “Two-Dimensional Covalent  
52 Organic Framework: Synthesis and Applications”. Grant number NRF-CRP16-2015-02,  
53 funded by National Research Foundation, Prime Minister’s Office, Singapore. U.M.  
54 acknowledges the support from Singapore National Research Foundation (NRF-CRP16-  
55 2015-05).  
56  
57  
58  
59  
60

## Reference

1. Huang, N.; Wang, P.; Jiang, D. Covalent organic frameworks: a materials platform for structural and functional designs. *Nat. Rev. Mater.* **2016**, *1*, 16068.
2. Segura, J. L.; Mancheno, M. J.; Zamora, F. Covalent organic frameworks based on Schiff-base chemistry: synthesis, properties and potential applications. *Chem. Soc. Rev.* **2016**, *45*, 5635-5671.
3. Diercks, C. S.; Yaghi, O. M. The atom, the molecule, and the covalent organic framework. *Science* **2017**, *355*, eaal1585.
4. Lyle, S. J.; Waller, P. J.; Yaghi, O. M. Covalent Organic Frameworks: Organic Chemistry Extended into Two and Three Dimensions. *Trends in Chemistry* **2019**, *1*, 172-184.
5. Jiang, D.; Chen, X.; Geng, K.; Liu, R.; Tan, K. T.; Gong, Y.; Li, Z.; Tao, S.; Jiang, Q. Covalent Organic Frameworks: Chemical Approaches to Designer Structures and Built-in Functions. *Angew. Chem., Int. Ed.* **2019**, *58*, 2-44.
6. Kandambeth, S.; Dey, K.; Banerjee, R. Covalent Organic Frameworks: Chemistry beyond the Structure. *J. Am. Chem. Soc.* **2019**, *141*, 1807-1822.
7. Côté, A. P.; Benin, A. I.; Ockwig, N. W.; O'Keeffe, M.; Matzger, A. J.; Yaghi, O. M. Porous, Crystalline, Covalent Organic Frameworks. *Science* **2005**, *310*, 1166-1170.
8. Evans, A. M.; Parent, L. R.; Flanders, N. C.; Bisbey, R. P.; Vitaku, E.; Kirschner, M. S.; Schaller, R. D.; Chen, L. X.; Gianneschi, N. C.; Dichtel, W. R. Seeded growth of single-crystal two-dimensional covalent organic frameworks. *Science* **2018**, eaar7883.
9. El-Kaderi, H. M.; Hunt, J. R.; Mendoza-Cortes, J. L.; Cote, A. P.; Taylor, R. E.; O'Keeffe, M.; Yaghi, O. M. Designed synthesis of 3D covalent organic frameworks. *Science* **2007**, *316*, 268-272.
10. Ma, T.; Kapustin, E. A.; Yin, S. X.; Liang, L.; Zhou, Z.; Niu, J.; Li, L.-H.; Wang, Y.; Su, J.; Li, J.; Wang, X.; Wang, W. D.; Wang, W.; Sun, J.; Yaghi, O. M. Single-crystal x-ray diffraction structures of covalent organic frameworks. *Science* **2018**, *361*, 48.
11. Liu, Y.; Ma, Y.; Zhao, Y.; Sun, X.; Gándara, F.; Furukawa, H.; Liu, Z.; Zhu, H.; Zhu, C.; Suenaga, K.; Oleynikov, P.; Alshammari, A. S.; Zhang, X.; Terasaki, O.; Yaghi, O. M. Weaving of organic threads into a crystalline covalent organic framework. *Science* **2016**, *351*, 365-369.
12. Liu, Y.; Diercks, C. S.; Ma, Y.; Lyu, H.; Zhu, C.; Alshimmri, S. A.; Alshihri, S.; Yaghi, O. M. 3D Covalent Organic Frameworks of Interlocking 1D Square Ribbons. *J. Am. Chem. Soc.* **2019**, *141*, 677-683.
13. Biswal Bishnu, P.; Chaudhari Harshal, D.; Banerjee, R.; Kharul Ulhas, K. Chemically Stable Covalent Organic Framework (COF)-Polybenzimidazole Hybrid Membranes: Enhanced Gas Separation through Pore Modulation. *Chem. Eur. J.* **2016**, *22*, 4695-4699.
14. Kang, Z.; Peng, Y.; Qian, Y.; Yuan, D.; Addicoat, M. A.; Heine, T.; Hu, Z.; Tee, L.; Guo, Z.; Zhao, D. Mixed Matrix Membranes (MMMs) Comprising Exfoliated 2D Covalent Organic Frameworks (COFs) for Efficient CO<sub>2</sub> Separation. *Chem. Mater.* **2016**, *28*, 1277-1285.
15. Fan, H.; Mundstock, A.; Feldhoff, A.; Knebel, A.; Gu, J.; Meng, H.; Caro, J. Covalent Organic Framework-Covalent Organic Framework Bilayer Membranes for Highly Selective Gas Separation. *J. Am. Chem. Soc.* **2018**, *140*, 10094-10098.
16. DeBlase, C. R.; Silberstein, K. E.; Truong, T.-T.; Abruña, H. D.; Dichtel, W. R.  $\beta$ -Ketoenamine-Linked Covalent Organic Frameworks Capable of Pseudocapacitive Energy Storage. *J. Am. Chem. Soc.* **2013**, *135*, 16821-16824.

17. Xu, F.; Jin, S.; Zhong, H.; Wu, D.; Yang, X.; Chen, X.; Wei, H.; Fu, R.; Jiang, D. Electrochemically active, crystalline, mesoporous covalent organic frameworks on carbon nanotubes for synergistic lithium-ion battery energy storage. *Sci. Rep.* **2015**, *5*, 8225.
18. Wang, S.; Wang, Q.; Shao, P.; Han, Y.; Gao, X.; Ma, L.; Yuan, S.; Ma, X.; Zhou, J.; Feng, X.; Wang, B. Exfoliation of Covalent Organic Frameworks into Few-Layer Redox-Active Nanosheets as Cathode Materials for Lithium-Ion Batteries. *J. Am. Chem. Soc.* **2017**, *139*, 4258-4261.
19. Li, X.; Gao, Q.; Wang, J.; Chen, Y.; Chen, Z.-H.; Xu, H.-S.; Tang, W.; Leng, K.; Ning, G.-H.; Wu, J.; Xu, Q.-H.; Quek, S. Y.; Lu, Y.; Loh, K. P. Tuneable near white-emissive two-dimensional covalent organic frameworks. *Nat. Commun.* **2018**, *9*, 2335.
20. Gao, Q.; Li, X.; Ning, G.-H.; Leng, K.; Tian, B.; Liu, C.; Tang, W.; Xu, H.-S.; Loh, K. P. Highly photoluminescent two-dimensional imine-based covalent organic frameworks for chemical sensing. *Chem. Commun.* **2018**, *54*, 2349-2352.
21. Albacete, P.; Martínez, J. I.; Li, X.; López-Moreno, A.; Mena-Hernando, S. a.; Platero-Prats, A. E.; Montoro, C.; Loh, K. P.; Pérez, E. M.; Zamora, F. Layer-Stacking-Driven Fluorescence in a Two-Dimensional Imine-Linked Covalent Organic Framework. *J. Am. Chem. Soc.* **2018**, *140*, 12922-12929.
22. Haldar, S.; Chakraborty, D.; Roy, B.; Banappanavar, G.; Rinku, K.; Mullangi, D.; Hazra, P.; Kabra, D.; Vaidhyanathan, R. Anthracene-Resorcinol Derived Covalent Organic Framework as Flexible White Light Emitter. *J. Am. Chem. Soc.* **2018**, *140*, 13367-13374.
23. Ding, S. Y.; Gao, J.; Wang, Q.; Zhang, Y.; Song, W. G.; Su, C. Y.; Wang, W. Construction of Covalent Organic Framework for Catalysis: Pd/COF-LZU1 in Suzuki-Miyaura Coupling Reaction. *J. Am. Chem. Soc.* **2011**, *133*, 19816-19822.
24. Fang, Q.; Gu, S.; Zheng, J.; Zhuang, Z.; Qiu, S.; Yan, Y. 3D Microporous Base-Functionalized Covalent Organic Frameworks for Size-Selective Catalysis. *Angew. Chem., Int. Ed.* **2014**, *53*, 2878-2882.
25. Lin, S.; Diercks, C. S.; Zhang, Y.-B.; Kornienko, N.; Nichols, E. M.; Zhao, Y.; Paris, A. R.; Kim, D.; Yang, P.; Yaghi, O. M.; Chang, C. J. Covalent organic frameworks comprising cobalt porphyrins for catalytic CO<sub>2</sub> reduction in water. *Science* **2015**, *349*, 1208-1213.
26. Vyas, V. S.; Haase, F.; Stegbauer, L.; Savasci, G.; Podjaski, F.; Ochsenfeld, C.; Lotsch, B. V. A tunable azine covalent organic framework platform for visible light-induced hydrogen generation. *Nat. Commun.* **2015**, *6*, 8508.
27. Xu, H.; Gao, J.; Jiang, D. Stable, crystalline, porous, covalent organic frameworks as a platform for chiral organocatalysts. *Nat. Chem.* **2015**, *7*, 905-912.
28. Chandra, S.; Kundu, T.; Kandambeth, S.; BabaRao, R.; Marathe, Y.; Kunjir, S. M.; Banerjee, R. Phosphoric Acid Loaded Azo (-N=N-) Based Covalent Organic Framework for Proton Conduction. *J. Am. Chem. Soc.* **2014**, *136*, 6570-6573.
29. Xu, H.; Tao, S.; Jiang, D. Proton conduction in crystalline and porous covalent organic frameworks. *Nat. Mater.* **2016**, *15*, 722-726.
30. Montoro, C.; Rodríguez-San-Miguel, D.; Polo, E.; Escudero-Cid, R.; Ruiz-González, M. L.; Navarro, J. A. R.; Ocón, P.; Zamora, F. Ionic Conductivity and Potential Application for Fuel Cell of a Modified Imine-Based Covalent Organic Framework. *J. Am. Chem. Soc.* **2017**, *139*, 10079-10086.
31. Du, Y.; Yang, H.; Whiteley, J. M.; Wan, S.; Jin, Y.; Lee, S.-H.; Zhang, W. Ionic Covalent Organic Frameworks with Spiroborate Linkage. *Angew. Chem., Int. Ed.* **2016**, *55*, 1737-1741.
32. Li, X.; Loh, K. P. Recent Progress in Covalent Organic Frameworks as Solid-State Ion Conductors. *ACS Materials Letters* **2019**, *1*, 327-335.

- 1  
2  
3 33. Li, X.; Gao, Q.; Aneesh, J.; Xu, H.-S.; Chen, Z.; Tang, W.; Liu, C.; Shi, X.; Adarsh,  
4 K. V.; Lu, Y.; Loh, K. P. Molecular Engineering of Bandgaps in Covalent Organic  
5 Frameworks. *Chem. Mater.* **2018**, *30*, 5743-5749.
- 6 34. Biswal, B. P.; Valligatla, S.; Wang, M.; Banerjee, T.; Saad, N. A.; Mariserla, B. M. K.;  
7 Chandrasekhar, N.; Becker, D.; Addicoat, M.; Senkovska, I.; Berger, R.; Rao, D. N.; Kaskel,  
8 S.; Feng, X. Nonlinear Optical Switching in Regioregular Porphyrin Covalent Organic  
9 Frameworks. *Angew. Chem., Int. Ed.* **2019**, *58*, 6896-6900.
- 10 35. Rowan Stuart, J.; Cantrill Stuart, J.; Cousins Graham, R. L.; Sanders Jeremy, K. M.;  
11 Stoddart, J. F. Dynamic Covalent Chemistry. *Angew. Chem., Int. Ed.* **2002**, *41*, 898-952.
- 12 36. Feng, X.; Ding, X.; Jiang, D. Covalent organic frameworks. *Chem. Soc. Rev.* **2012**, *41*,  
13 6010-6022.
- 14 37. Ascherl, L.; Sick, T.; Margraf, J. T.; Lapidus, S. H.; Calik, M.; Hettstedt, C.;  
15 Karaghiosoff, K.; Döblinger, M.; Clark, T.; Chapman, K. W.; Auras, F.; Bein, T. Molecular  
16 docking sites designed for the generation of highly crystalline covalent organic frameworks.  
17 *Nat. Chem.* **2016**, *8*, 310-316.
- 18 38. Dalapati, S.; Jin, E.; Addicoat, M.; Heine, T.; Jiang, D. Highly Emissive Covalent  
19 Organic Frameworks. *J. Am. Chem. Soc.* **2016**, *138*, 5797-5800.
- 20 39. Smith, B. J.; Dichtel, W. R. Mechanistic Studies of Two-Dimensional Covalent  
21 Organic Frameworks Rapidly Polymerized from Initially Homogenous Conditions. *J. Am.*  
22 *Chem. Soc.* **2014**, *136*, 8783-8789.
- 23 40. Matsumoto, M.; Dasari, R. R.; Ji, W.; Feriante, C. H.; Parker, T. C.; Marder, S. R.;  
24 Dichtel, W. R. Rapid, Low Temperature Formation of Imine-Linked Covalent Organic  
25 Frameworks Catalyzed by Metal Triflates. *J. Am. Chem. Soc.* **2017**, *139*, 4999-5002.
- 26 41. Karak, S.; Kandambeth, S.; Biswal, B. P.; Sasmal, H. S.; Kumar, S.; Pachfule, P.;  
27 Banerjee, R. Constructing Ultraporous Covalent Organic Frameworks in Seconds via an  
28 Organic Terracotta Process. *J. Am. Chem. Soc.* **2017**, *139*, 1856-1862.
- 29 42. Guan, X.; Ma, Y.; Li, H.; Yusran, Y.; Xue, M.; Fang, Q.; Yan, Y.; Valtchev, V.; Qiu,  
30 S. Fast, Ambient Temperature and Pressure Ionothermal Synthesis of Three-Dimensional  
31 Covalent Organic Frameworks. *J. Am. Chem. Soc.* **2018**, *140*, 4494-4498.
- 32 43. Uribe-Romo, F. J.; Doonan, C. J.; Furukawa, H.; Oisaki, K.; Yaghi, O. M. Crystalline  
33 Covalent Organic Frameworks with Hydrazone Linkages. *J. Am. Chem. Soc.* **2011**, *133*,  
34 11478-11481.
- 35 44. Stegbauer, L.; Schwinghammer, K.; Lotsch, B. V. A hydrazone-based covalent  
36 organic framework for photocatalytic hydrogen production. *Chem. Sci.* **2014**, *5*, 2789-2793.
- 37 45. Liu, W.; Su, Q.; Ju, P.; Guo, B.; Zhou, H.; Li, G.; Wu, Q. A Hydrazone-Based  
38 Covalent Organic Framework as an Efficient and Reusable Photocatalyst for the  
39 Cross-Dehydrogenative Coupling Reaction of N-Aryltetrahydroisoquinolines. *ChemSusChem*  
40 **2016**, *10*, 664-669.
- 41 46. Ding, S.-Y.; Dong, M.; Wang, Y.-W.; Chen, Y.-T.; Wang, H.-Z.; Su, C.-Y.; Wang, W.  
42 Thioether-Based Fluorescent Covalent Organic Framework for Selective Detection and  
43 Facile Removal of Mercury(II). *J. Am. Chem. Soc.* **2016**, *138*, 3031-3037.
- 44 47. Gottschling, K.; Stegbauer, L.; Savasci, G.; Prisco, N. A.; Berkson, Z. J.; Ochsenfeld,  
45 C.; Chmelka, B. F.; Lotsch, B. V. Molecular Insights into Carbon Dioxide Sorption in  
46 Hydrazone-Based Covalent Organic Frameworks with Tertiary Amine Moieties. *Chem.*  
47 *Mater.* **2019**, *31*, 1946-1955.
- 48 48. Zhang, G.; Hong, Y.-I.; Nishiyama, Y.; Bai, S.; Kitagawa, S.; Horike, S.  
49 Accumulation of Glassy Poly(ethylene oxide) Anchored in a Covalent Organic Framework as  
50 a Solid-State Li<sup>+</sup> Electrolyte. *J. Am. Chem. Soc.* **2019**, *141*, 1227-1234.
- 51  
52  
53  
54  
55  
56  
57  
58  
59  
60

- 1  
2  
3 49. Li, X.; Wang, H.; Chen, Z.; Xu, H.-S.; Yu, W.; Liu, C.; Wang, X.; Zhang, K.; Xie, K.;  
4 Loh, K. P. Covalent-Organic-Framework-Based Li-CO<sub>2</sub> Batteries. *Adv. Mater.* **2019**, *31*,  
5 1905879.  
6  
7 50. Kandambeth, S.; Shinde, D. B.; Panda, M. K.; Lukose, B.; Heine, T.; Banerjee, R.  
8 Enhancement of Chemical Stability and Crystallinity in Porphyrin-Containing Covalent  
9 Organic Frameworks by Intramolecular Hydrogen Bonds. *Angew. Chem., Int. Ed.* **2013**, *52*,  
10 13052-13056.  
11  
12 51. Chen, X.; Addicoat, M.; Jin, E.; Zhai, L.; Xu, H.; Huang, N.; Guo, Z.; Liu, L.; Irlle, S.;  
13 Jiang, D. Locking Covalent Organic Frameworks with Hydrogen Bonds: General and  
14 Remarkable Effects on Crystalline Structure, Physical Properties, and Photochemical Activity.  
15 *J. Am. Chem. Soc.* **2015**, *137*, 3241-3247.  
16  
17 52. Guo, X.; Tian, Y.; Zhang, M.; Li, Y.; Wen, R.; Li, X.; Li, X.; Xue, Y.; Ma, L.; Xia, C.;  
18 Li, S. Mechanistic Insight into Hydrogen-Bond-Controlled Crystallinity and Adsorption  
19 Property of Covalent Organic Frameworks from Flexible Building Blocks. *Chem. Mater.*  
20 **2018**, *30*, 2299-2308.  
21  
22 53. Halder, A.; Karak, S.; Addicoat, M.; Bera, S.; Chakraborty, A.; Kunjattu Shebeeb, H.;  
23 Pachfule, P.; Heine, T.; Banerjee, R. Ultrastable Imine-Based Covalent Organic Frameworks  
24 for Sulfuric Acid Recovery: An Effect of Interlayer Hydrogen Bonding. *Angew. Chem., Int.*  
25 *Ed.* **2018**, *57*, 5797-5802.  
26  
27

## TOC

